Chemical Engineering Journal, Volume 367, 1 July 2019, pp. 249-259
DOI: 10.1016/j.cej.2019.02.123

Silver Nanoparticles Confined in Shell-in-Shell Hollow TiO_2 Manifesting Efficiently Photocatalytic Activity and Stability

Shidong Zhao [a], Juanrong Chen [b]*, Yifei Liu[a], Ying Jiang,[c] Caiguo Jiang [a], Zhengliang Yin [a],Yingguan Xiao[a], Shunsheng Cao [a,c]*

[a]*Institute of Polymer Materials, School of Materials Science and Engineering, Jiangsu University, Zhenjiang 212013, China*

[b]*School of Environment and Safety Engineering, Jiangsu University, Zhenjiang 212013, China*

[c]*School of Water, Energy and Environment, Cranfield University, Bedford MK43 0AL, UK*

Abstract: The complete degradation of tetracycline still is a challenge for TiO_2-based photocatalysts under simulated solar light irradiation. To tackle this challenge, we devise Ag nanoparticles (Ag NPs) confined in shell-in-shell hollow TiO_2 photocatalyst (HTAT). This strategy mainly involves the construction of CPS@TiO_2 core-shell composites, the form of TiO_2 inner shell, AgNPs loading by photo-deposition, the assembly of TiO_2 outer shell, and phase transition of anatase TiO_2 by calcination at 450℃. All characterizations including TEM, STEM Mapping, BET, and XPS confirm the unique structure of the as-synthesized HTAT photocatalyst. As expected, the complete degradation of tetracycline (TC and TCH) can be realized by using HTAT photocatalyst under simulated solar light irradiation because its TiO_2 two shells simultaneously take part in the photodegrading reaction of TC or TCH. The transformation intermediates and degradation pathway were analyzed by LC/MS. Our work effectively overcomes the disadvantages of many previously reported TiO_2-based photocatalysts for the incomplete degradation of tetracycline.

Keywords: TiO_2-Ag@TiO_2; shell-in-shell hollow TiO_2; tetracycline; confined effect; degradation mechanism

1. Introduction

∗ Corresponding authors.
E-mail addresses: chenjuanrong@ujs.edu.cn (J. Chen), sscaochem@hotmail.com, sscao@ujs.edu.cn (S. Cao).

The abuse of tetracycline has led to a series of environmental problems due to its high toxicity, persistence and carcinogenicity. [1-3] TiO_2-assisted photocatalytic degradation has been considered as an efficient method for the removal of organic pollutants due to its strong oxidizing ability. [4,5] For example, Du et al [6] synthesized three-dimensional porous CdS/TiO_2 with 67.1% degradation rate of tetracycline (TC) under visible light irradiation. Wang et al [7] reported that as-synthesized Au-TiO_2 hold visible-degradation (74%) of TC. Yang et al [8] used TiO_2 microtubes as visible-light photocatalyst and obtained 76% removal rate of TC under visible-light irradiation. Unfortunately, it is still very difficult in achieving efficient or complete degradation of TC for TiO_2-based photocatalysts due to the unique macromolecular ring structure of TC. [1, 9, 10]

Various strategies have been introduced to enhance removal rate of TC. For example, Shi et al [11] reported that Cu_2O-TiO_2 composite exhibited a 88.81% removal rate of tetracycline hydrochloride under simulated solar light irradiation. Shao et al [12] prepared three-dimensional Ag_3PO_4/TiO_2@MoS_2 photocatalyst with high photodegradation rate (92%) of TC under 800 w xenon arc lamp irradiation. Ahmadi et al [13] reported that the remove of TC was as high as 100% under UV light irradiation for MWCNT/TiO_2 photocatalyst. Clearly, intense light source is very efficient method to achieve high degradation rate of TC. Compared with UV light irradiation, simulated solar-light-driven photocatalytic process is a green technology for sewage treatment. [14] However, it is still a challenge for completely degrading TC via TiO_2-based photocatalysts under simulated solar light irradiation. [11,15-17] Therefore, the novel design is very important in exploring TiO_2-based photocatalysts for the complete degradation of tetracycline. Recently, our group successfully constructed SiO_2-Ag@TiO_2 composite with enhanced catalytic efficiency for degrading TC in comparison with directly immobilizing silver nanoparticles onto the surface of TiO_2 by introducing confined effect. [18] However, it is still hard to achieve complete removal of TC because SiO_2 itself

does not take part in the photocatalytic process. [19]

In this work, we present the first attempt to explore new TiO_2 photocatalyst with an excellent photocatalytic activity and reusability by using Ag NPs confined in shell-in-shell hollow TiO_2 (HTAT). The hollow/porous structure of as-synthesized photocatalyst not only boosts the diffusion of reactants by lowering diffusion resistance, but also traps incident light for a long time and achieves high efficiency for photon utilization. Furthermore, the introduction of confined effect can exhibit higher efficiency towards the degradation of pollutants because Ag NPs are used as "linker" between TiO_2 two shells. Compared with TiO_2 single shell and SiO_2@TiO_2 hybrid shell, more importantly, the as-synthesized photocatalyst can take full advantages of TiO_2 two shells by introducing Ag NPs as "electron reservoir and electron transfer channel", substantially improving separation efficiency of photogenerated e^-/h^+ pairs. As a result, the as-synthesized HTAT photocatalyst manifests complete removal of tetracycline (TC and TCH) and excellent recyclability, opening a new pathway for constructing other semiconductor photocatalysts with shell-in-shell structure.

2. Experimental

2.1. Materials

Tetrabutyl titanate was obtained from J&K Chemical Technology. Styrene (St), tetracycline (TC), tetracycline hydrochloride (TCH), and absolute ethanol were available from Sinopharm Chemical Reagent Co., Ltds and were used without purification except styrene that was removed inhibitor with sodium hydroxide (5wt.%).

2.2. Synthesis of hollow TiO_2 inner shell (HT).

The CPS@TiO_2 spheres were synthesized according to our previous works [20,21] and then the CPS template was calcined at 300 °C for 10 h to prepare hollow TiO_2 inner shell.

2.3. Ag nanoparticles (Ag NPs) loading

Photo-deposition has been widely used to prepare TiO_2-supported metal NPs. [22] Typically, 350 mg of HT was dispersed into 5% of ethanol aqueous solution (50 mL), followed by addition of glycerol (6.3g) and $AgNO_3$ (8mg), subsequently, the system was purged with N_2 for 1h. After irradiation of simulated sunlight (XHA350 W, 350 W) for 5h, the suspension was centrifuged, washed and dried at 80 °C, obtaining hollow TiO_2-Ag spheres.

2.4. Preparation of Ag NPs confined in shell-in-shell hollow TiO_2 photocatalyst (HTAT)

The hollow TiO_2-Ag was modified with ATS and further coated by using TBT (1g) under H_2O (3 ml) to generate TiO_2 outer shell, finally the photocatalyst was obtained by calcined at 450 ℃ and reduction with $NaBH_4$.

2.5. Characterization

Transmission electron microscope (TEM), scanning electron microscope (SEM), and STEM Mapping were used to measure the architecture of as-synthesized HTAT. In addition, Energy dispersive X-ray (EDX), XRD, XPS, and UV–vis spectroscopy were used to characterize crystal, bonding energy and absorption spectrum of TiO_2-Ag@TiO_2 spheres.

2.6. Photodegrading experiment

The photocatalytic efficiency of the HTAT were investigated towards the degradation of tetracycline (TC) and tetracycline hydrochloride (TCH) aqueous solution (20 mg/L, 50 ml) using HTAT as photocatalyst (0.1 mg/ml) under visible light (λ >420 nm) or simulated solar light (350W Xe lamp) irradiation. The suspension was magnetically stirred for 30 min in dark to ensure the establishment of adsorption equilibrium before light irradiation. Finally, 3 mL samples were withdrawn from the degradation system, then centrifuged and analyzed by UV–vis spectra (λ= ~357 nm).[23, 24]

3. Results and discussion

3.1. The construction and characterization of TiO_2-Ag@TiO_2

Scheme 1 briefly demonstrated the design ideas and synthetic pathway of TiO_2-Ag@TiO_2. Firstly, CPS@TiO_2 colloidal spheres (white powders) were synthesized according to our previous publication. [20,21] After that, CPS was removed by calcination at 300℃ to prepare hollow TiO_2 inner shell. Secondly, under light illumination, Ag NPs was loaded on the surface of hollow TiO_2 inner shell through photo-deposition technique, forming brown TiO_2-Ag spheres. Subsequently, TiO_2-Ag was further coated through sol-gel reaction of TBT, producing TiO_2-Ag@TiO_2 precursors. Finally, the gray TiO_2-Ag@TiO_2 photocatalyst was formed after calcination at 450 °C and reduced by $NaBH_4$.

Scheme 1. Formation pathway of hollow TiO_2-Ag@TiO_2 photocatalyst

Fig. 1 displays TEM and SEM images of HTAT. As demonstrated in Fig. 1a, the obvious difference of gray scale shows the hollow nature of HTAT. Further closer observation of the TEM image suggests that the overlap of TiO_2 two shells indicated by red arrows is able to be seen. Such shell-in-shell hollow TiO_2 structure is further confirmed by a higher magnification TEM image of HTAT (Fig. 1b). On the other hand, the typical SEM image (Fig. 1c) of broken spheres also demonstrates the hollow nature of the as-synthesized HTAT. Moreover, there are many black dots (Ag NPs) homogeneously anchored to the TiO_2 inner shell in each HTAT sphere, as shown in Fig. 1a,b. The average size of Ag NPs is ~5.83 nm evaluated from the images (Fig.1a,b), which facilitates photo-generated electron transfer and boosts photocatalytic process. [18]

EDX analysis was applied to measure chemical composition distribution of HTAT. Fig. 2 indicates that Ti and O signals are presented in the form of whole HTAT sphere, while the Ag signal (deep red) is mainly dispersed in the HTAT spheres. Compared with the same condensation steps of single

hollow TiO_2 (HT) in N_2 adsorption and desorption, [25] the as-synthesized HTAT exhibits a representative type IV curve (Fig. 1d), suggesting a shell-in-shell structure. Further observation reveals that HTAT possess a higher specific surface area (~75.9m^2/g), which is twice higher than that of HT (~32.7 m^2/g). All these results confirm that the HTAT photocatalyst with a shell-in-shell structure has been successfully prepared.

Fig .1. TEM (a, b), SEM (c) images of HTAT and (d) N_2 adsorption/desorption isotherms of HTAT**,** HT, and the pore-size distribution of HTAT (insert).

Fig 2. EDX spectrum of areas (a), STEM image (b) and EDX mapping of the HTAT photocatalyst (d: Ti, e: O, f: Ag, and g: C).

3.2. Crystal structure characterization

The crystal structure of HTAT photocatalyst is analyzed by the powder X-ray diffraction (XRD), as shown in Fig 3**.** There are five diffraction peaks located at 2θ = 25.3°, 38°, 48.1°, 62.8°, 75.2°, which are consistent with (101), (004), (200), (204), (215) crystal planes of anatase (JCPDS: 21-1272), respectively. [26,27] Incidentally, the peaks of Ag NPs are not seen in HTAT because of the low proportion (~1.1wt.%) of Ag NPs in the HTAT, indicating that the peaks corresponding to Ag NPs is not able to be distinguished in the dominating TiO_2 patterns because of much stronger peaks' intensities of TiO_2.[28,44]

Fig.3 XRD patterns of TiO_2-Ag@TiO_2 spheres

3.3. XPS analysis and UV–vis spectra of HTAT

X-ray photo-electron spectroscopy (XPS) was used to study the chemical states of the elements in the HTAT. Fig. 4a shows the existence of O, Ti, Ag and C in the form of O1s, Ti2p, Ag3d, and C1s. Fig. 4b exhibits Ti2p spectrum of HTAT. The peaks located at 458.51 and 464.29eV are attributed to $Ti2p_{3/2}$ and $Ti2p_{1/2}$, [27] a positively shift of (~0.3 eV) of $Ti2p_{3/2}$ and (~0.57 eV) of $Ti2p_{1/2}$ can be found for HTAT compared with the corresponding binding energies of P25 (458.21 and 463.72 eV). The increase in the binding energies may be ascribed to the action between Ag NPs, carbon and host TiO_2. Fig. 4c shows the XPS spectrum of O1s, there is a peak at 530.1 eV related to the bulk oxygen bound of TiO_2. Also, the peak at 533.2 eV is responsible for hydroxyl groups adsorbed onto the surface of TiO_2. [20,27] In the case of Ag3d (Fig. 4d), the symmetrical peaks at 367.3 and 373.3eV can be ascribed to the $Ag3d_{5/2}$ and $Ag3d_{3/2}$, respectively, the spin energy separation of the Ag 3d doublet is 6.0 eV, indicating that Ag is in good agreement with metallic Ag. [22,29] The peaks centered at 284.84, 286.31 and 288.77 eV in C1s spectrum are indicated as C-C, C=O and C-O-Ti bonds, respectively (Fig. 4e). The peak at 284.84 eV is attributed to the vestigial carbon, while other peaks are designated as the existence of oxygen bound substances in HTAT spheres.[18,20]

Fig. 4. (a) Full-scale XPS spectra of HTAT, (b) Ti2p, (c) O1s, (d) Ag 3d, (e) C1s for HTAT sample.

The UV–vis absorbance data provide a clear evidence that Ag NPs was anchored on HTAT photocatalyst. The Ag nanoparticles loaded on the surface of single-shelled hollow TiO_2 (HTA) and P25 were used as reference photocatalysts, as shown in Fig. 5. The absorption edge of P25 is at 400 nm, which is in a good agreement with the intrinsic band energy of pure TiO_2 (~3.2 eV). [30] After the immobilization of Ag NPs , the resulted HTA shows a visible-light absorption range due to the surface plasmon resonance effect[31]. In addition, the as-synthesized HTAT exhibits the strongest

visible-light absorption (400-600 nm) compared with HTA and P25.

Fig. 5. UV-vis absorption spectra of the HTAT, HTA and P25

3.4. Photocatalytic degradation of TC under visible- light irradiation

Under visible light irradiation, the photocatalytic performance of as-synthesized HTAT was measured by degrading TC. The silver NPs loaded on the surface of hollow TiO_2 spheres (HTA) and hollow TiO_2 spheres (HT) were employed as reference photocatalysts, as shown in Fig. 6. Fig.6a indicates that the removal rate of TC is almost negligible after visible-light irradiation, suggesting that TC itself is extremely hard to be mineralized. [32] After 40 min irradiation, HT photocatalyst can degrade ~24.1% TC, slightly below the removal value (~32.4%) of TC for HTA photocatalyst because of the surface plasmon resonance of Ag NPs. By contrast, the as-synthesized HTAT photocatalyst exhibits the highest degradation rate of TC (~70%) under the same photocatalytic conditions (40 min) because of confined effect and TiO_2 two shells. [18] Even if the extension of time (120 min) is used, the removal rate of TC is only ~58% for HTA photocatalyst, indicating that HTAT exhibits three times faster degradation rate of TC than traditional HTA photocatalyst. [18] Furthermore, the photocatalytic efficiency of HTAT was further compared with similar-structured SiO_2-Ag@TiO_2 (HSAT) photocatalyst by referring our previously work. [18] Under the same experimental conditions, the degradation rate of TC achieves a significant improvement for as-synthesized HTAT because it can take full advantages of TiO_2 two shells via Ag NPs linkage.

Fig 6. Photocatalytic performances of HTAT, HTA and HT (a), and HSAT, HTAT (b) for visible-light degradation of TC

3.5. Photocatalytic degradation of TC under simulated solar light irradiation

As afore-mentioned, we expect that the as-synthesized HTAT photocatalyst can completely degrade tetracycline under simulated solar light irradiation, effectively working out the incomplete degradation of tetracycline for TiO_2-based photocatalysts.[16] Therefore, the degradation experiment of TC was further investigated for HTAT photocatalyst under simulated solar light irradiation, while HTA and HT were also used as reference photocatalysts, as demonstrated in Fig. 7. Compared with the visible-light removal rate of TC, the value of TC is slightly increased to 8.8% after 100 min irradiation, further confirming that TC itself is very hard to be degraded even under simulated solar light irradiation. [24,33] The removal rates of TC for HT and HTA photocatalysts are further increased to 86% and 95.2% under the same photocatalytic conditions, respectively. Excitedly, the HTAT photocatalyst can exhibit 99.9% TC removal efficiency, indicating that TC has been completely degraded under simulated solar light irradiation. The excellently photocatalytic efficiency is further confirmed by degrading tetracycline hydrochloride (TCH), as demonstrated in Fig.7b. Compared with the degradation of TC, the removal rate of TCH for HTA photocatalyst slightly decreases to ~91.8% after 80 min irradiation (simulated solar light), while as-synthesized HTAT still exhibits a complete degradation (100%) of TCH under the same condition. The photocatalytic results strongly confirm that the HTAT manifests excellent photocatalytic efficiency towards the degradation of tetracycline (TC or TCH), effectively overcoming the disadvantages of many previously reported TiO_2-based photocatalysts for the incomplete degradation of tetracycline. [11,15-17]

Fig 7. Photocatalytic activity of HTAT, HTA and HT for simulated solar-light degradation of TC (a) and TCH (b)

3.6. Role of active oxidative species

To ascertain main active oxidative species towards the degradation of TC, trapping experiments

were carried out by adding various scavengers such as nitrogen (N_2), 1mmol of t-butanol (t-BuOH) and 1mmol of triethanolamine (TEOA). [6,34,35] As shown in Fig 8, the addition of N_2 substantially restrains the light activity of HTAT, indicating that $\bullet O^{2-}$ is crucial active specie for TC degradation.[6] When TEOA is added, a decrease in degradation rate (~80.6%) of TC is obtained, indicating that h^+ is also main active specie under photodegrading process. [34] By contrast, the addition of t-BuOH does not cause the obviously change for the removal rate of TC, suggesting that •OH does not play a positive role for the photocatalytic reaction. [35]

Fig .8. Photocatalytic performances of HTAT for degrading TC in the existence of trapping agents

3.7. TC photodegradation Mechanism and Pathway

To study the photocatalytic mechanism of HTAT, charge separation efficiency was investigated by testing transient photocurrent response and using EIS Nyquist plots . **Fig.9**a shows that HTAT exhibits an enhanced photocurrent intensity than HTA under simulated solar light irradiation, indicating the higher transfer efficiency of photogenerated charges for HTAT **[1, 4]**. This is further confirmed by a much smaller semicircle in the Nyquist plots, as shown in Fig.9b. Additionally, time-resolved transient photoluminescence (PL) spectroscopy was used to analyse the survival time of photogenerated pairs of HTAT and HTA. As shown in Fig.9c, the transient PL decay trace of the HTAT shows a PL lifetime of ~10.28ns, while the PL lifetime for HTA attains ~7.23 ns. The longer PL lifetime of HTAT suggests that HTAT manifests the faster separation of electron/hole pairs **[45]**. These results provide clear evidence that the confinement effect of Ag NPs, which links the two TiO_2 shells and act as electron reservoirs and electron transfer channels, inhibit the charge recombination and prolong the lifetime of charge carriers.

To further clarify the photocatalytic degradation mechanism of TC by HTAT, the electron spin resonance (ESR) spin-trapping with DMPO was conducted under simulated solar light irradiation to detect radicals generated during the catalytic processes. Fig. 10a shows that each system has four characteristic peaks with intensity ratio of 1:2:2:1 for DMPO-·OH adducts, indicating the generation of ·OH radicals. The intensive of DMPO-·OH peaks when HTAT was applied was significantly stronger compared to HTA. This indicates that more ·OH are produced after irradiation which is in agreement with previous studies **[45,46]**. More importantly, Fig.10b indicates that HTAT resulted in higher $\bullet O_2^-$ signal intensity, which is in agreement with the free radicals trapping experiments. Therefore, the ESR spin-trapping results confirmed that Ag NPs confined in shell-in-shell hollow TiO_2 (HTAT) photocatalyst products more radicals to degrade TC under simulated solar light irradiation. The conclusion is in accordance with the results of TC degradation efficiency and PL spectra.

Fig. 10 ESR spectra of (a) DMPO-·OH adduct and (b) DMPO-$\bullet O_2^-$ adduct over HTAT and HTA.

Based on photoelectrochemical properties and experimental evidences, a probable degradation-mechanism according to unique shell-in-shell structure of HTAT was proposed in this work, as demonstrated in **Sheme.2**. Ag NPs serves as light harvester and produces many electrons under visible-light irradiation. Whist photo-generated electrons can be fast migrated onto the surfaces of the inner and outer TiO_2 shells because Ag NPs can be acted as electron transfer channel, and thus reduce the dissolved O_2 easily, resulting in an improved degradation rate of TC.

Under simulated solar light irradiation, two TiO_2 shells both are excited and generate lots of h^+/e^- pairs, subsequently, the photo-induced electrons rapidly migrate into the Ag NPs “reservoirs”, considerably improving the separation efficiency of h^+/e^- pairs (Fig.9 and Fig.10)**,** meanwhile, the

high oxidation power of holes left behind in the deep level of TiO_2 can directly degrade TC, [36] which agrees well with the fact that h^+ is also main active specie under photodegrading process (**Fig**.8). Therefore, two TiO_2 shells can simultaneously take part in the photodegrading reaction of TC because of the "bridge" of Ag NPs, resulting in complete degradation of TC. By contrast, hollow TiO_2 or SiO_2@TiO_2 hybrid photocatalyst only utilizes TiO_2 single shell, resulting in the incomplete removal of TC. Compared with previously reported TiO_2-based photocatalysts, moreover, the larger surface area, more photocatalytic active sites, and higher utilization rate of incident light due to the shell-in-shell structure and two TiO_2 shells of HTAT also play positive roles for the degradation of TC.

Scheme 2. Mechanism of photocatalytic degradation

To obtain the degradation pathway of TC, photodegradation intermediates were detected by MS during the photocatalytic process, as shown in **Fig**.11. The product with m/z =445 was ascribed to the molecular weight of TC. Unlike ·OH oxidation mechanism and pathway [37,38], Possible two main degradation pathways of TC by $\cdot O_2^-$ were proposed because the larger intermediates with m/z=461 or 475 generated by hydroxylation reaction were not detected in this study, indicating that •OH did not play a positive role for the photocatalytic reaction, as demonstrated in **Fig**.8. After simulative sunlight irradiation, the N-methyl group of TC molecule were lost, producing the product 1 (m/z=416) [39]. Subsequently, the carboatomic ring or acylamino in product 1 was cleaved to generate product 2 (m/z=333) and product 3 (m/z=345). Because of the strong oxidizing $\cdot O_2^-$, the product 2 and 3 could be further oxidized to gain an intermediate with m/z=305 (product 4) and m/z=303 (product 5), respectively. [40,41] The product 6 (m/z=260) and product 7 (m/z=279) were detected by losing the carboxyl group or methanol in carboatomic ring under further attacked by $\cdot O_2^-$. Owing to the open-ring reactions and the loss of some functional groups, some small molecular organics such as acids

and alcohols could be generated due to further degradation of intermediates. Finally, CO_2, H_2O and inorganic ions were ultimately converted in the HTAT system.

Fig.11. The proposed photodegradation pathways of TC

3.8. Recyclability of TiO_2-Ag@TiO_2 photocatalyst

It has been proved that metal nanoparticles modified TiO_2 photocatalysts hold good recyclability under photodegrading process**.** [42,43] However, such recyclability can be obtained only under mild conditions.[18] In principle, the as-synthesized HTAT photocatalyst should offer superior recyclability even under very harsh conditions because Ag NPs is tightly protected by TiO_2 two shells, considerably enhancing its practical potential. To confirm the hypothesis, a reusability experiment for the degradation of TC was conducted under simulated solar irradiation using HTAT and HTA photocatalysts. After each photodegrading experiment, the sample was separated, stirred with HCl (3mol/L solution, 45ml) for 2h, rinsed and dried under UV light (GHX-2-300W) irradiation and then reused for the next test.

Fig.12a illustrates that HTAT still can degrade TC completely even after five recycling runs, implying that HTAT possess an extremely photocatalytic stability for the removal of tetracycline in wastewater. By contrast, the degradation rate of TC catalyzed by the HTA decreases significantly from 95.2% to 79% in the second cycle. Interestingly, the degradation rate of TC does not further drop with the increase in number of cycles, which is mainly ascribed to the photocatalytic activity of TiO_2 itself because Ag NPs may be corroded completely after HCl treatment. Although HT photocatalyst presents a lower degradation rate of TC (86%) that HTA in first photodegrading test, the same value (Fig.12b) is obtained for HTA and HT after the second cycle, indicating that the

activity of Ag NPs for HTA photocatalyst has lost completely after HCl treatment. The results strongly confirm that the as-synthesized HTAT exhibits a superior recyclability after HCl treatment, substantially broadening its practical potential, especially for the degradation of acidic antibiotics such as TCH.

Fig. 12. Cycling tests for the degradation of TC using HTAT, HTA and HT photocatalyst

4. Conclusion

In summary, we explore Ag NP confined in shell-in-shell hollow TiO_2 photocatalyst. During the photodegrading process, TiO_2 two shells can simultaneously participate in the photocatalytic reaction by introducing Ag NPs as "electron reservoir and electron transfer channel" between TiO_2 two shells. As a result, the HTAT photocatalyst exhibits an increased visible-light catalytic efficiency towards the degradation of TC in comparison with hollow TiO_2, Ag modified TiO_2, and SiO_2-Ag@TiO_2 photocatalysts. Excitedly, the complete removal and excellent recyclability of tetracycline can be achieved by using HTAT as photocatalyst under simulated light irradiation because of its unique shell-in-shell structure and confined effect. Therefore, the as-synthesized HTAT opens a new window for the design and construction of other semiconductor photocatalysts with two shells.

Acknowledgments

Financial supports of this research from the National Natural Science Foundation of China (Grants 21876069, 21707054), the Six Talent Peaks Project in Jiangsu (XCL-018), China Postdoctoral Science Foundation (No. 2016M601744), and the China Scholarship Council (CSC) .

References

[1] Y. Gong, Y. Wu, Y. Xu, L. Li, C. Li, X. Liu, L. Niu. All-solid-state Z-scheme CdTe/TiO_2 heterostructure photocatalysts with enhanced visible-light photocatalytic degradation of antibiotic waste water. Chem. Eng. J, 350 (2018) 257–267.

[2] Y. Yang, Z. Zeng, C. Zhang, D. Huang, G. Zeng, R. Xiao, C. Lai, C. Zhou, H. Guo, W. Xue, M. Cheng, W. Wang, J. Wang, Construction of iodine vacancy-rich BiOI/Ag@AgI Z-scheme heterojunction photocatalysts for visible-light-driven tetracycline degradation: Transformation pathways and mechanism insight, Chem. Eng. J, 349 (2018) 808-82.

[3] X.J. Lu, Y. Wang, X.Y. Zhang, G.Q. Xu, D.M. Wang, J. Lv, Z.X. Zheng, Y.C. Wu, NiS and MoS_2 nanosheet co-modified graphitic C_3N_4 ternary heterostructure for high efficient visible light photodegradation of antibiotic, J Hazard Mater, 341 (2018) 10-19.

[4] X. Feng, P. Wang, J. Hou, J. Qian, Y. Ao, C. Wang. Significantly enhanced visible light photocatalytic efficiency of phosphorus doped TiO_2 with surface oxygen vacancies for ciprofloxacin degradation: Synergistic effect and intermediates analysis. J. Hazard. Mater, 351 (2018) 196-205

[5]. Y. Nie, F. Yu, L. Wang, Q. Xing, X. Liu, Y. Pei, J. Zou, W. Dai, Y. Li, S. L. Suib, Photocatalytic degradation of organic pollutants coupled with simultaneous photocatalytic H_2 evolution over Graphene quantum dots/Mn-N-TiO_2/g-C_3N_4 composite catalysts: performance and mechanism, Appl. Catal. B-Environ., 227 (2018) 312-321

[6] Y.B. Du, L. Zhang, M. Ruan, C.G. Niu, X.J. Wen, C. Liang, X.G. Zhang, G.M. Zeng, Template-free synthesis of three-dimensional porous CdS/TiO_2 with high stability and excellent visible photocatalytic activity, Mater Chem Phys, 212 (2018) 69-77.

[7] C. Wang, Y.L. Wu, J. Lu, J. Zhao, J.Y. Cui, X.L. Wu, Y.S. Yan, P.W. Huo, Bioinspired Synthesis of Photocatalytic Nanocomposite Membranes Based on Synergy of Au-TiO_2 and Polydopamine for Degradation of Tetracycline under Visible Light, ACS Appl Mater Interface, 9 (2017) 23687-23697.

[8] L. Yang, X. Li, Z.R. Wang, Y. Shen, M. Liu, Natural fiber templated TiO_2 microtubes via a double soaking sol-gel route and their photocatalytic performance, Appl Surf Sci, 420 (2017) 346-354.

[9] B.F. Luo, D.B. Xu, D. Li, G.L. Wu, M.M. Wu, W.D. Shi, M. Chen, Fabrication of a Ag/Bi_3TaO_7 Plasmonic Photocatalyst with Enhanced Photocatalytic Activity for Degradation of Tetracycline, ACS Appl Mater Interface, 7 (2015) 17061-17069.

[10] Y. Liu, J.J. Kong, J.L. Yuan, W. Zhao, X. Zhu, C. Sun, J.M. Xie, Enhanced photocatalytic activity over flower-like sphere $Ag/Ag_2CO_3/BiVO_4$ plasmonic heterojunction photocatalyst for tetracycline degradation, Chem Eng J, 331 (2018) 242-254.

[11] Y. Shi, Z. Yang, B. Wang, H. An, Z. Chen, H. Cui, Adsorption and photocatalytic degradation of tetracycline hydrochloride using a palygorskite-supported Cu_2O-TiO_2 composite, Appl Clay Sci, 119 (2016) 311-320.

[12] N. Shao, J.N. Wang, D.D. Wang, P. Corvini, Preparation of three-dimensional $Ag_3PO_4/TiO_2@MoS_2$ for enhanced visible-light photocatalytic activity and anti-photocorrosion, Appl Catal B-Environ, 203 (2017) 964-978.

[13] M. Ahmadi, H.R. Motlagh, N. Jaafarzadeh, A. Mostoufi, R. Saeedi, G. Barzegar, S. Jorfi, Enhanced photocatalytic degradation of tetracycline and real pharmaceutical wastewater using MWCNT/TiO_2 nano-composite, J Environ Manage, 186 (2017) 55-63.

[14] S. Bagheri, A. TermehYousefi, T.-O. Do, Photocatalytic pathway toward degradation of environmental pharmaceutical pollutants: structure, kinetics and mechanism approach, Catal Sci Technol, 7 (2017) 4548-4569.

[15] C. Zhao, M. Pelaez, X.D. Duan, H.P. Deng, K. O'Shea, D. Fatta-Kassinos, D.D. Dionysiou, Role of pH on photolytic and photocatalytic degradation of antibiotic oxytetracycline in aqueous solution under visible/solar light: Kinetics and mechanism studies, Appl Catal B-Environ, 134 (2013) 83-92.

[16] L. Rimoldi, E. Pargoletti, D. Meroni, E. Falletta, G. Cerrato, F. Turco, G. Cappelletti, Concurrent role of metal (Sn, Zn) and N species in enhancing the photocatalytic activity of TiO_2 under solar light, Catal Today, 313 (2018) 40-46.

[17] L.-L. Qu, N. Wang, Y.-Y. Li, D.-D. Bao, G.-H. Yang, H.-T. Li, Novel titanium dioxide-graphene-activated carbon ternary nanocomposites with enhanced photocatalytic performance in rhodamine B and tetracycline hydrochloride degradation, J Mater Sci, 52 (2017) 8311-8320.

[18] Y. Zhang, J. Chen, H. Tang, Y. Xiao, S. Qiu, S. Li, S. Cao, Hierarchically-structured SiO_2-$Ag@TiO_2$ hollow spheres with excellent photocatalytic activity and recyclability, J Hazard Mater, 354 (2018) 17-26.

[19] D.M. Hu, Y.P. Huang, H. Liu, H. Wang, S.G. Wang, M.W. Shen, M.F. Zhu, X. Shi, The assembly of dendrimer-stabilized gold nanoparticles onto electrospun polymer nanofibers for catalytic applications, J. Mater. Chem. A, 2 (2014) 2323-2332.

[20] J. Shao, W. Sheng, M. Wang, S. Li, J. Chen, Y. Zhang, S. Cao, In situ synthesis of carbon-doped TiO_2 single-crystal nanorods with a remarkably photocatalytic efficiency, Appl Catal B-Environ, 209 (2017) 311-319.

[21] Y. Zhang, Y. Zhao, S. Cao, Z. Yin, L. Cheng, L. Wu. Design and Synthesis of Hierarchical SiO_2@C/TiO_2 Hollow Spheres for High-Performance Supercapacitors. ACS Appl. Mater. Interfaces 9 (2017) 29982−29991.

[22] N.L. Reddy, S. Kumar, V. Krishnan, M. Sathish, M.V. Shankar, Multifunctional Cu/Ag quantum dots on TiO_2 nanotubes as highly efficient photocatalysts for enhanced solar hydrogen evolution, J Catal, 350 (2017) 226-239.

[23] W. Shi, F. Guo, H. Wang, M. Han, H. Li, S. Yuan, H. Huang, Y. Liu, Z. Kang, Carbon dots decorated the exposing high-reactive (111) facets CoO octahedrons with enhanced photocatalytic activity and stability for tetracycline degradation under visible light irradiation, Appl. Catal. B-Environ, 219 (2017) 36-44.

[24] Y.Z. Hong, C.S. Li, G.Y. Zhang, Y.D. Meng, B.X. Yin, Y. Zhao, W.D. Shi, Efficient and stable Nb_2O_5 modified g-C_3N_4 photocatalyst for removal of antibiotic pollutant, Chem Eng J, 299 (2016)74-84.

[25] S. Cao, J. Chang, L. Fang, L. Wu, Metal Nanoparticles Confined in the Nanospace of Double-Shelled Hollow Silica Spheres for Highly Efficient and Selective Catalysis, Chem Mater, 28 (2016) 5596-5600.

[26] L. Cheng, S. Qiu, J. Chen, J. Shao, S. Cao. A practical pathway for the preparation of Fe_2O_3 decorated TiO_2 photocatalyst with enhanced visible-light photoactivity. Mate. Chem. Phys, 190 (2017) 53-61.

[27] Y Zhang, J. Chen, L. Hua, S. Li, X. Zhang, W. Sheng, S. Cao. High photocatalytic activity of hierarchical SiO_2@C-doped TiO_2 hollow spheres in UV and visible light towards degradation of Rhodamine B. J. Hazard. Mater, 340 (2017) 309–318.

[28] Y. Zhang, H. Ma, M. Yi, Z. Shen, X. Yu, X. Zhang, Magnetron-sputtering fabrication of noble metal nanodots coated TiO_2 nanoparticles with enhanced photocatalytic performance, Mater Design, 125 (2017) 94-99.

[29] X.S. Jiang, L. Pantanowitz, M.M. Bui, R. Esther, D. Budwit, L.G. Dodd, Clear Cell Chondrosarcoma: Cytologic Findings in Six Cases, Diagn Cytopathol, 42 (2014) 784-791.

[30] V. Likodimos, Photonic crystal-assisted visible light activated TiO_2 photocatalysis, Appl Catal

B-Environ, 230 (2018)269-303.

[31] Y. Wen, H. Ding, Y. Shan, Preparation and visible light photocatalytic activity of Ag/TiO2/graphene nanocomposite, Nanoscale, 3 (2011) 4411-4417.

[32] W. Shi, F. Guo, S. Yuan, In situ synthesis of Z-scheme $Ag_3PO_4/CuBi_2O_4$ photocatalysts and enhanced photocatalytic performance for the degradation of tetracycline under visible light irradiation, Appl Catal B-Environ, 209 (2017) 720-728.

[33] Z. Li, L.Y. Zhu, W. Wu, S.F. Wang, L.W. Qiang, Highly efficient photocatalysis toward tetracycline under simulated solar-light by Ag^+-CDs-Bi_2WO_6: Synergistic effects of silver ions and carbon dots, Appl Catal B-Environ, 192 (2016) 277-285.

[34] X. Lv, T. Wang, W. Jiang, Preparation of Ag@AgCl/g-C_3N_4/TiO_2 porous ceramic films with enhanced photocatalysis performance and self-cleaning effect, Ceram Int, 44 (2018) 9326-9337.

[35] W. Teng, X.Y. Li, Q.D. Zhao, J.J. Zhao, D.K. Zhang, In situ capture of active species and oxidation mechanism of RhB and MB dyes over sunlight-driven Ag/Ag_3PO_4 plasmonic nanocatalyst, Appl Catal B-Environ, 125 (2012) 538-545.

[36] A.T.O. Dal'Toe, G.L. Colpani, N. Padoin, M.A. Fiori, C. Soares, Lanthanum doped titania decorated with silver plasmonic nanoparticles with enhanced photocatalytic activity under UV-visible light, Appl Surf Sci, 441 (2018) 1057-1071.

[37] Z. Xie, Y. Feng, F. Wang, D. Chen, Q. Zhang, Y. Zeng, W. Lv, G. Liu, Construction of carbon dots modified MoO_3/g-C_3N_4 Z-scheme photocatalyst with enhanced visible-light photocatalytic activity for the degradation of tetracycline, Appl Catal B-Environ, 229 (2018) 96-104.

[38] T. Viet Ha Tran, B.-K. Lee, Great improvement on tetracycline removal using ZnO rod-activated carbon fiber composite prepared with a facile microwave method, J Hazard Mater, 324 (2017) 329-339.

[39] J. Cao, Z. Yang, W. Xiong, Y. Zhou, Y. Peng, X. Li, C. Zhou, R. Xu, Y. Zhang, One-step synthesis of Co-doped UiO-66 nanoparticle with enhanced removal efficiency of tetracycline: Simultaneous adsorption and photocatalysis, Chem Eng J, 353 (2018) 126-137.

[40] N. Tian, X. Tian, Y. Nie, C. Yang, Z. Zhou, Y. Li, Biogenic manganese oxide: An efficient peroxymonosulfate activation catalyst for tetracycline and phenol degradation in water, Chem Eng J, 352 (2018) 469-476

[41] X. Tang, L. Ni, J. Han, Y. Wang, Preparation and characterization of ternary magnetic g-C_3N_4 composite photocatalysts for removal of tetracycline under visible light, Chinese J Catal, 38 (2017)

447-457.

[42] P. Mazierski, A. Malankowska, M. Kobylanski, M. Diak, M. Kozak, M.J. Winiarski, T. Klimczuk, W. Lisowski, G. Nowaczyk, A. Zaleska-Medynska, Photocatalytically Active TiO_2/Ag_2O Nanotube Arrays Interlaced with Silver Nanoparticles Obtained from the One-Step Anodic Oxidation of Ti-Ag Alloys, ACS Catal, 7 (2017) 2753-2764.

[43] X. Feng, P. Wang, J. Jin, Q.Wang,Y.Ao. Oxygen vacancies and phosphorus codoped black titania coated carbon nanotube composite photocatalyst with efficient photocatalytic performance for the degradation of acetaminophen under visible light irradiation. Chem Eng J, 352 (2018) 947-956

[44] X. Jiang, Q. Xing, X. Luo, F. Li, J. Zou, S. Liu, X. Li, X. Wang. Simultaneous Photoreduction of Uranium(VI) and Photooxidation of Arsenic(III) In Aqueous Solution over g-C_3N_4/TiO_2 Heterostructured Catalysts under Simulated Sunlight Irradiation, Appl. Catal. B-Environ., 228 (2018) 29-38

[45] K. Wang, Y. Li, G. Zhang, J. Li, X. Wu. 0D Bi nanodots/2D Bi_3NbO_7 nanosheets heterojunctions for efficient visible light photocatalytic degradation of antibiotics: Enhanced molecular oxygen activation and mechanism insight. Appl. Catal. B-Environ., 240 (2019) 39–49

[46] Y. Yu, L. Yan, J. Cheng, C. Jing. Mechanistic insights into TiO_2 thickness in Fe_3O_4@TiO_2-GO composites for enrofloxacin photodegradation. Chemical Engineering Journal 325 (2017) 647–654

Figures

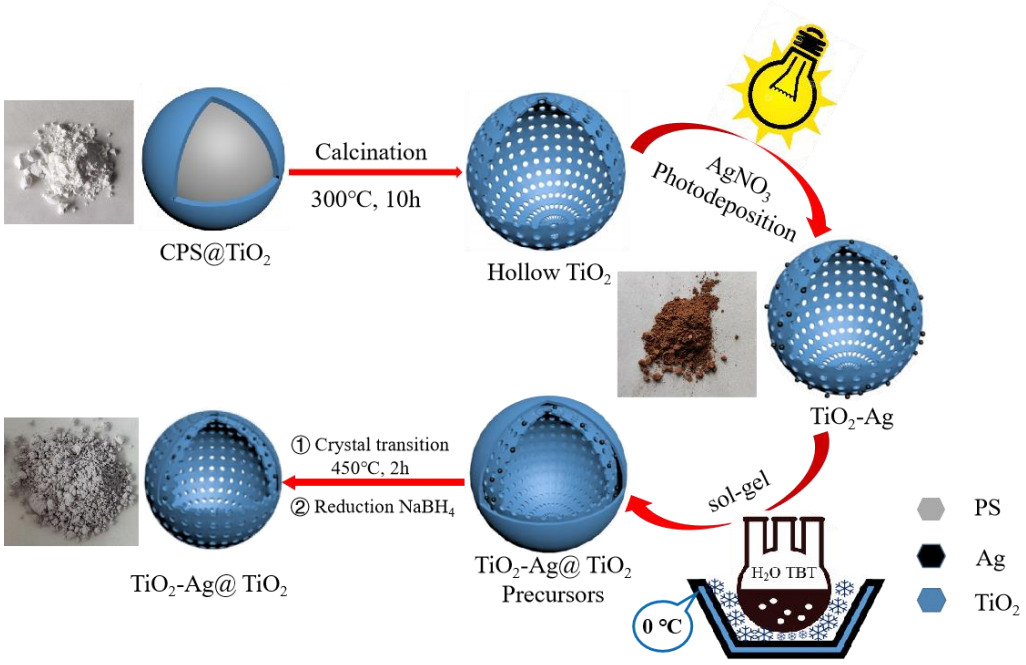

Scheme 1. Formation pathway of hollow TiO_2-Ag@TiO_2 photocatalyst

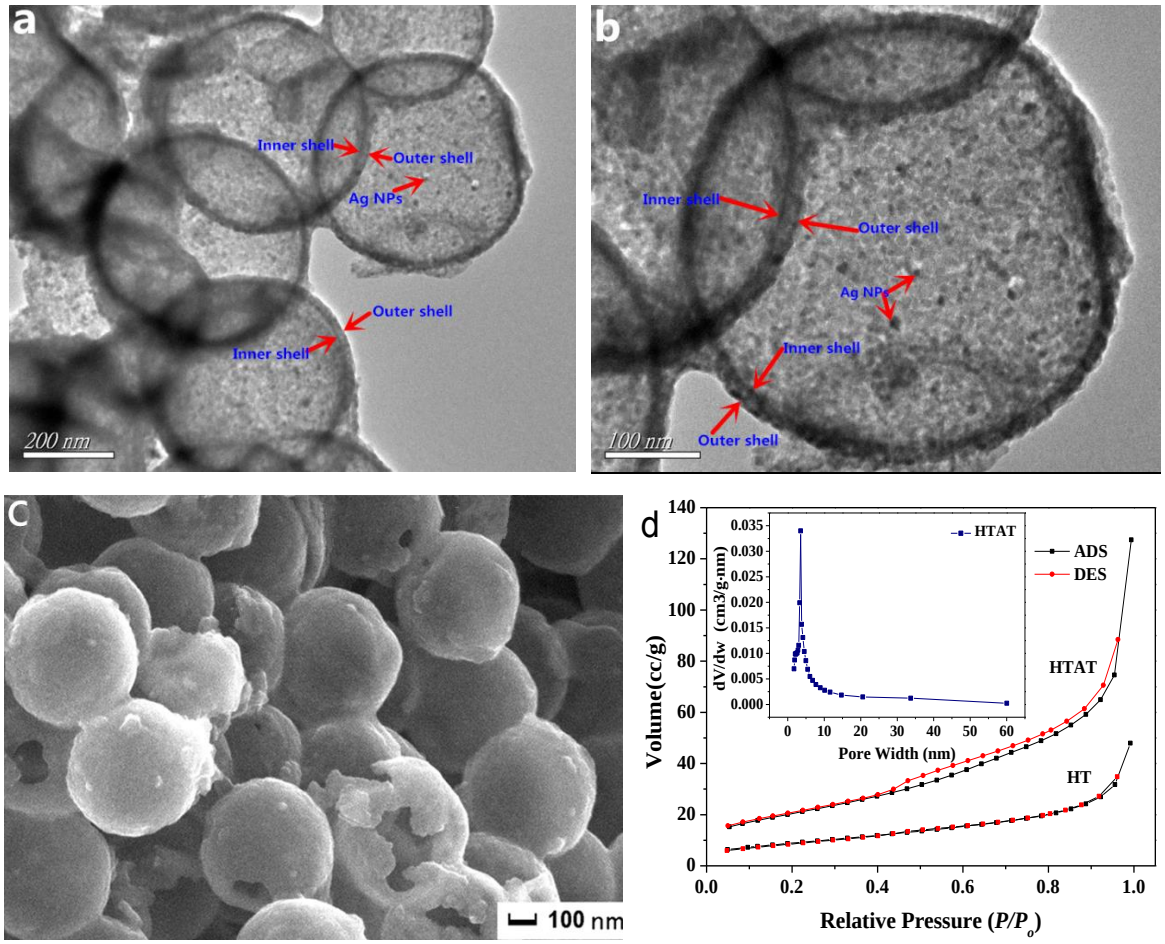

Fig .1. TEM (a, b), SEM (c) images of HTAT and (d) N_2 adsorption/desorption isotherms of HTAT， HT, and the pore-size distribution of HTAT (insert).

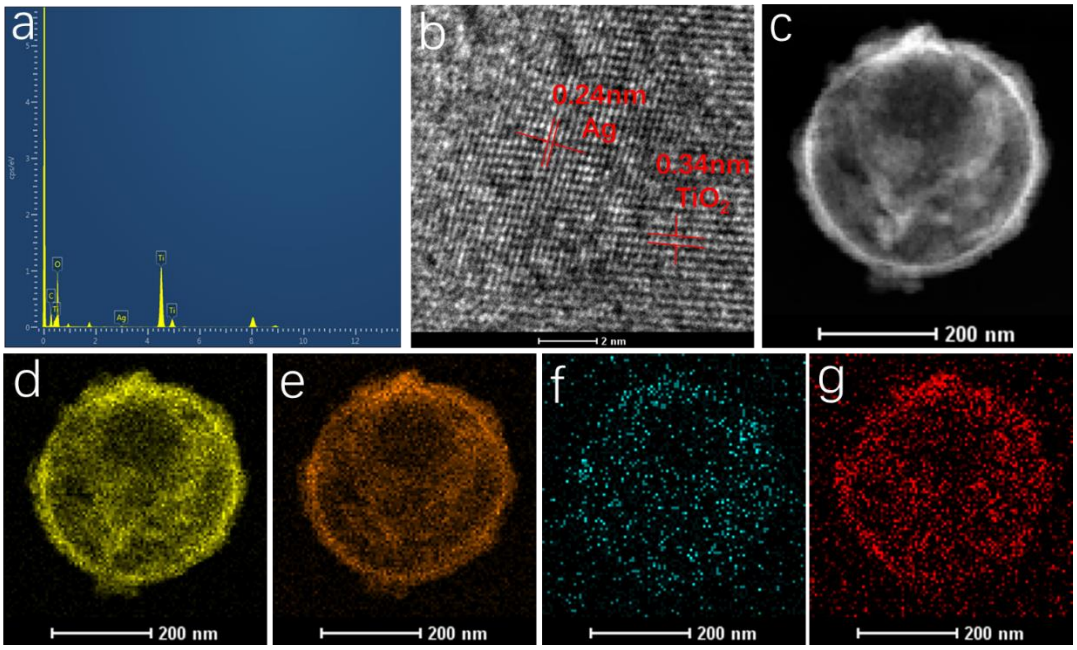

Fig 2. EDX spectrum of areas (a), STEM image (b) and EDX mapping of the HTAT photocatalyst (d: Ti, e: O, f: Ag, and g: C).

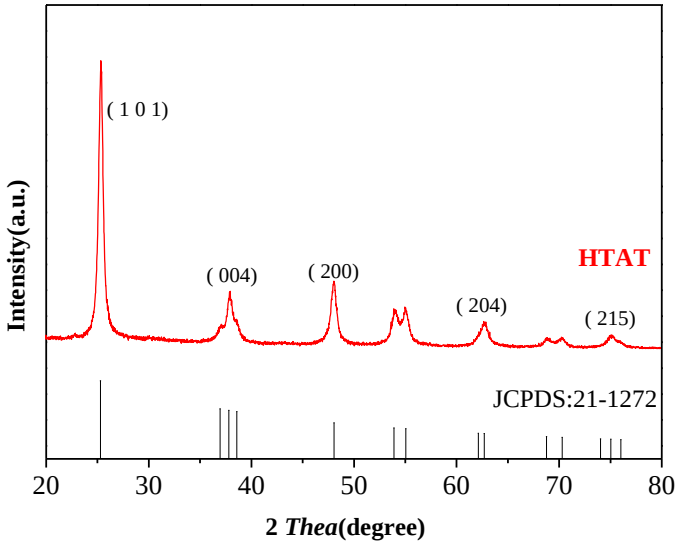

Fig.3 XRD patterns of TiO_2-Ag@TiO_2 spheres

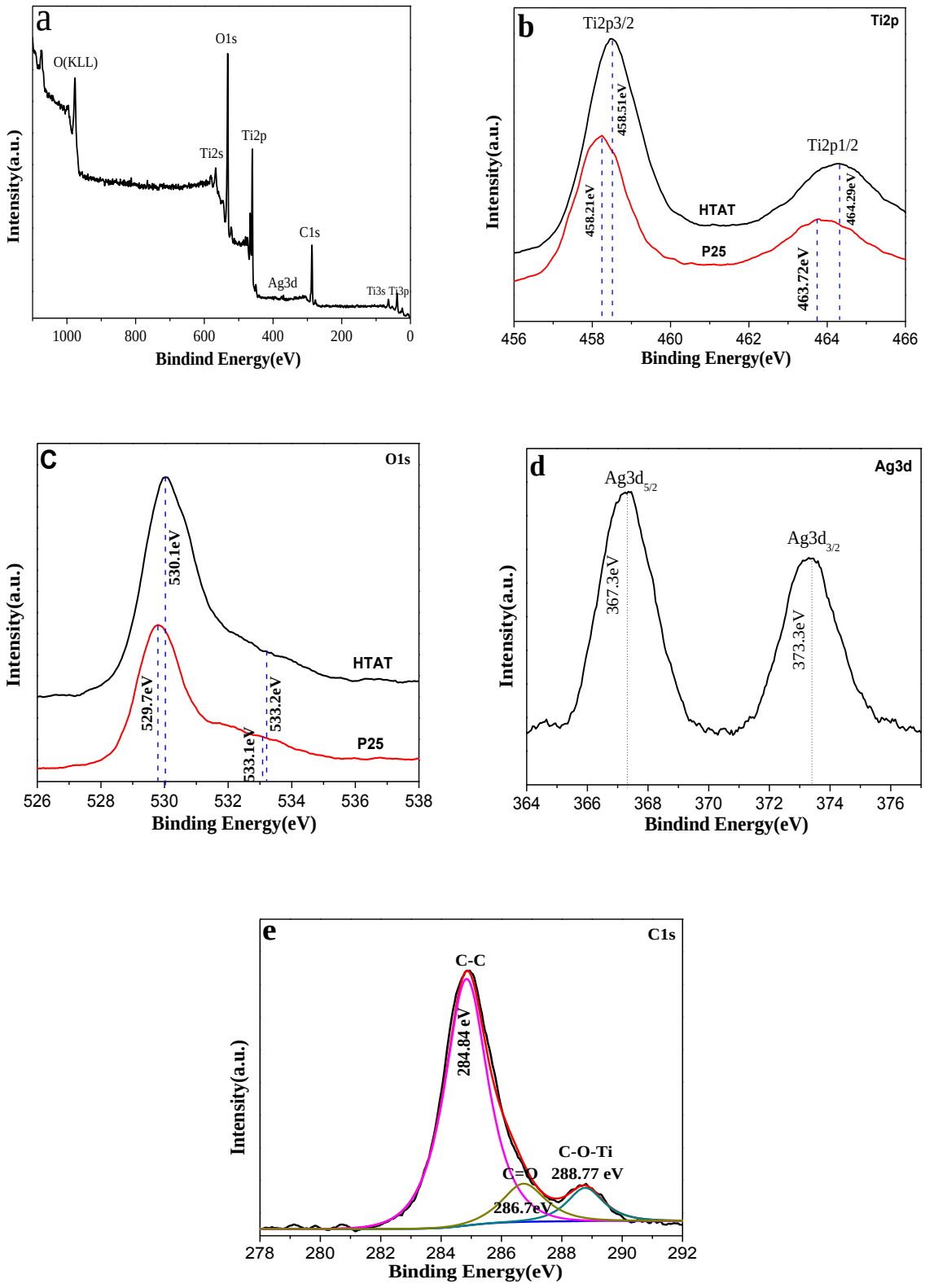

Fig. 4. (a) Full-scale XPS spectra of HTAT, (b) Ti2p, (c) O1s, (d) Ag 3d, (e) C1s for HTAT sample.

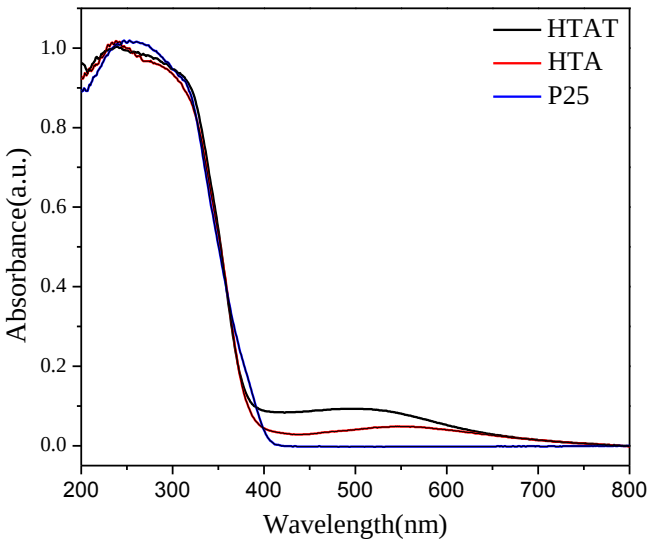

Fig. 5. UV-vis absorption spectra of the HTAT, HTA and P25

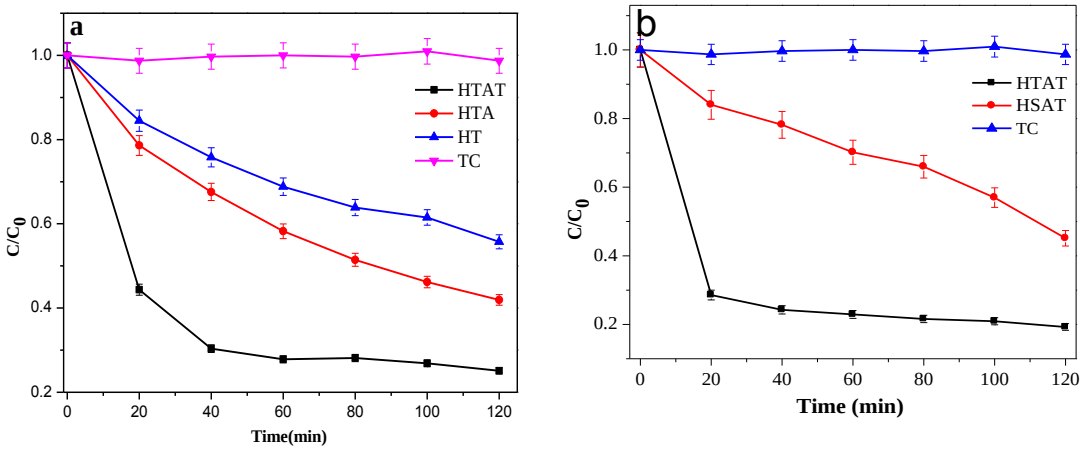

Fig 6. Photocatalytic performances of HTAT, HTA and HT (a), and HSAT, HTAT (b) for visible-light degradation of TC

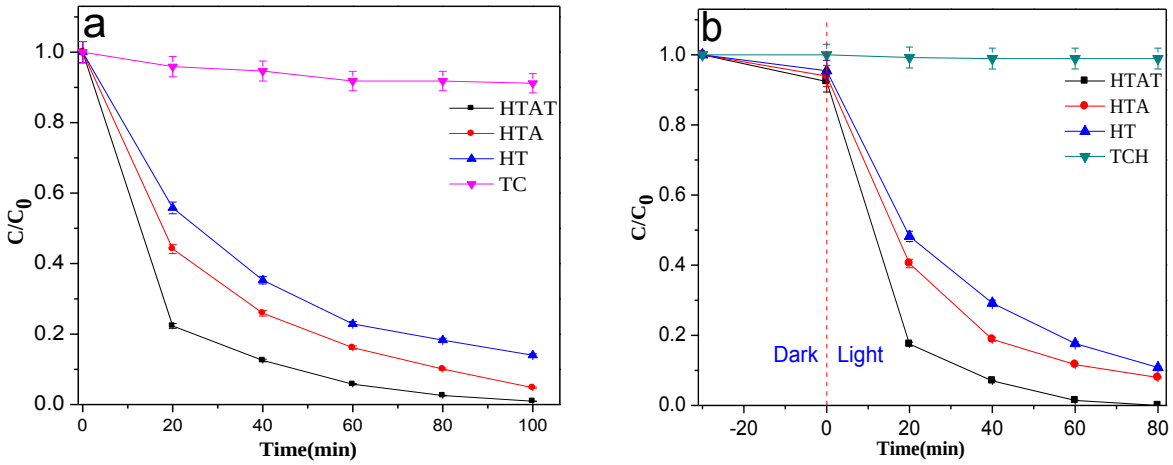

Fig 7. Photocatalytic activity of HTAT, HTA and HT for simulated solar-light degradation of TC (a) and TCH (b)

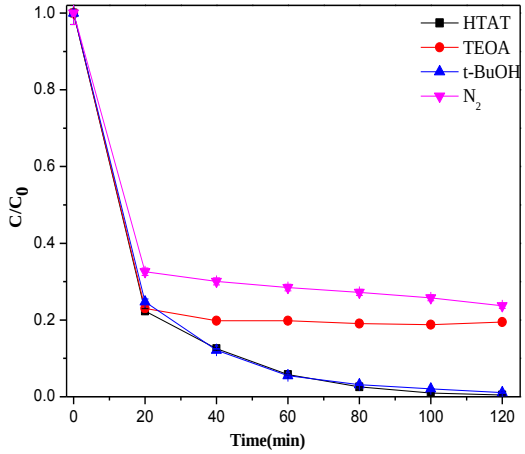

Fig .8. Photocatalytic performances of HTAT for degrading TC in the existence of trapping agents

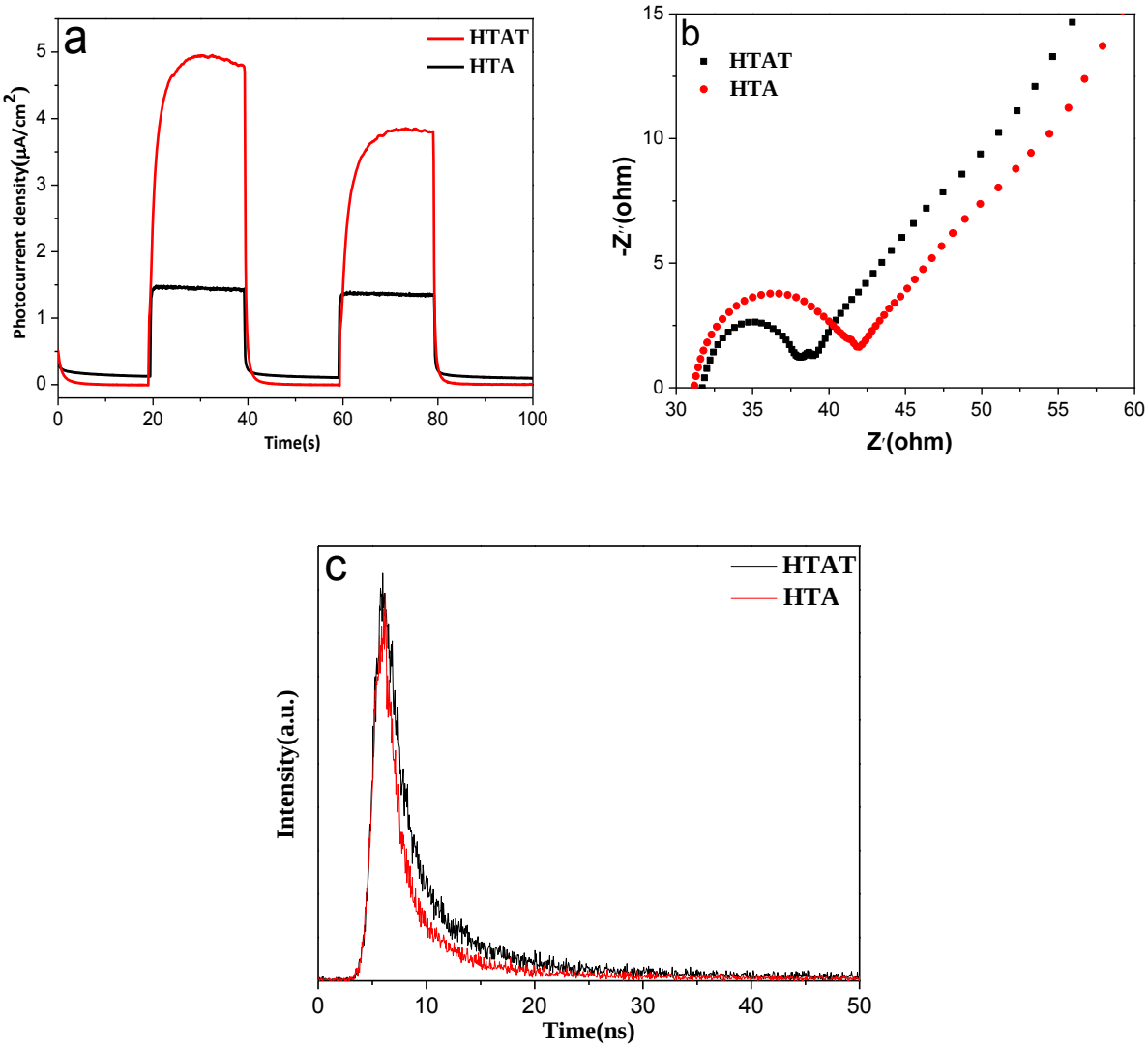

Fig. 9 (a) Transient photocurrent responses, (b) (EIS) and (c) photoluminescence decay traces of HTAT and HTA

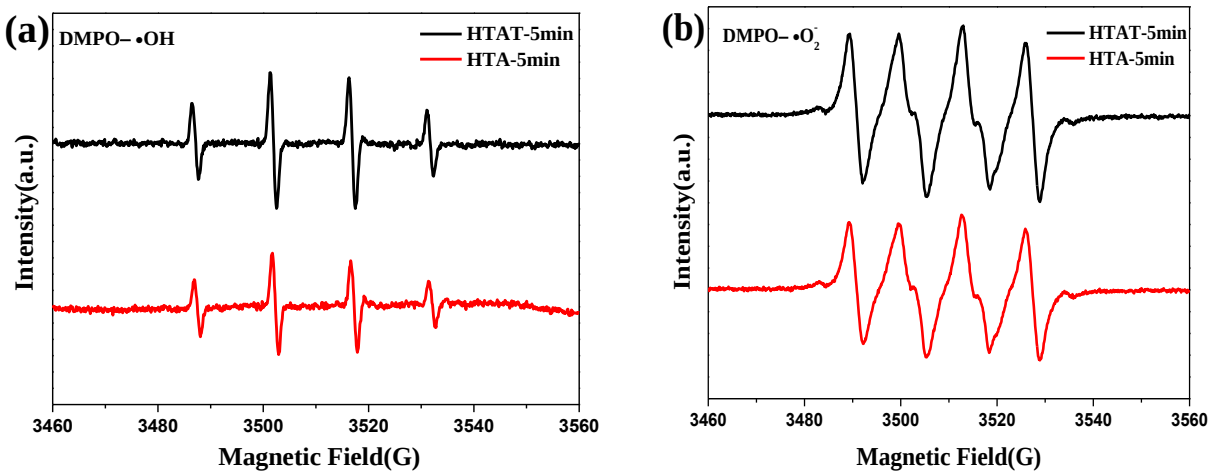

Fig. 10 ESR spectra of (a) DMPO-·OH adduct and (b) DMPO-•O_2^- adduct over HTAT and HTA

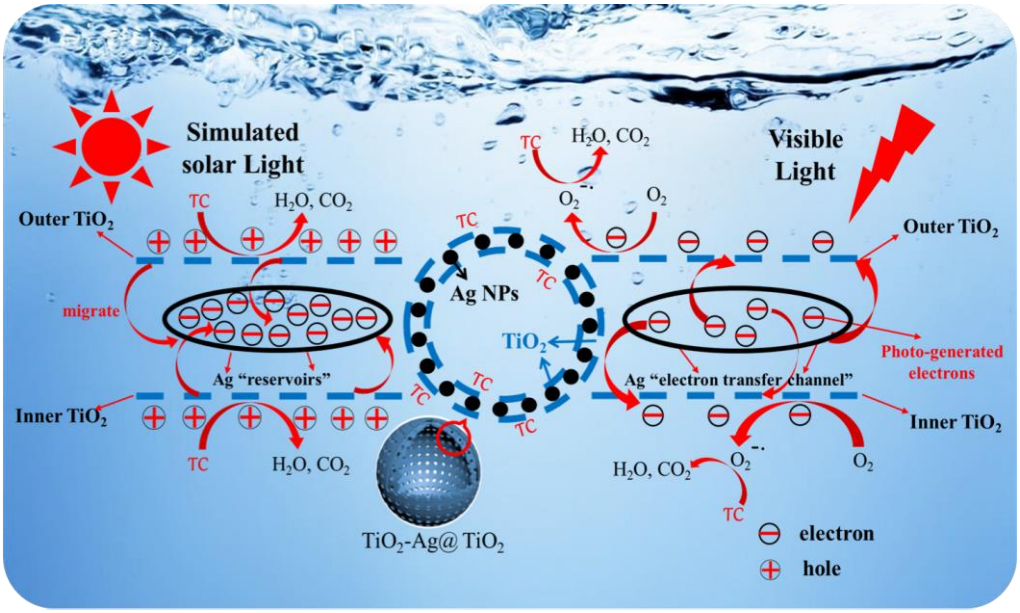

Scheme 2. Mechanism of photocatalytic degradation

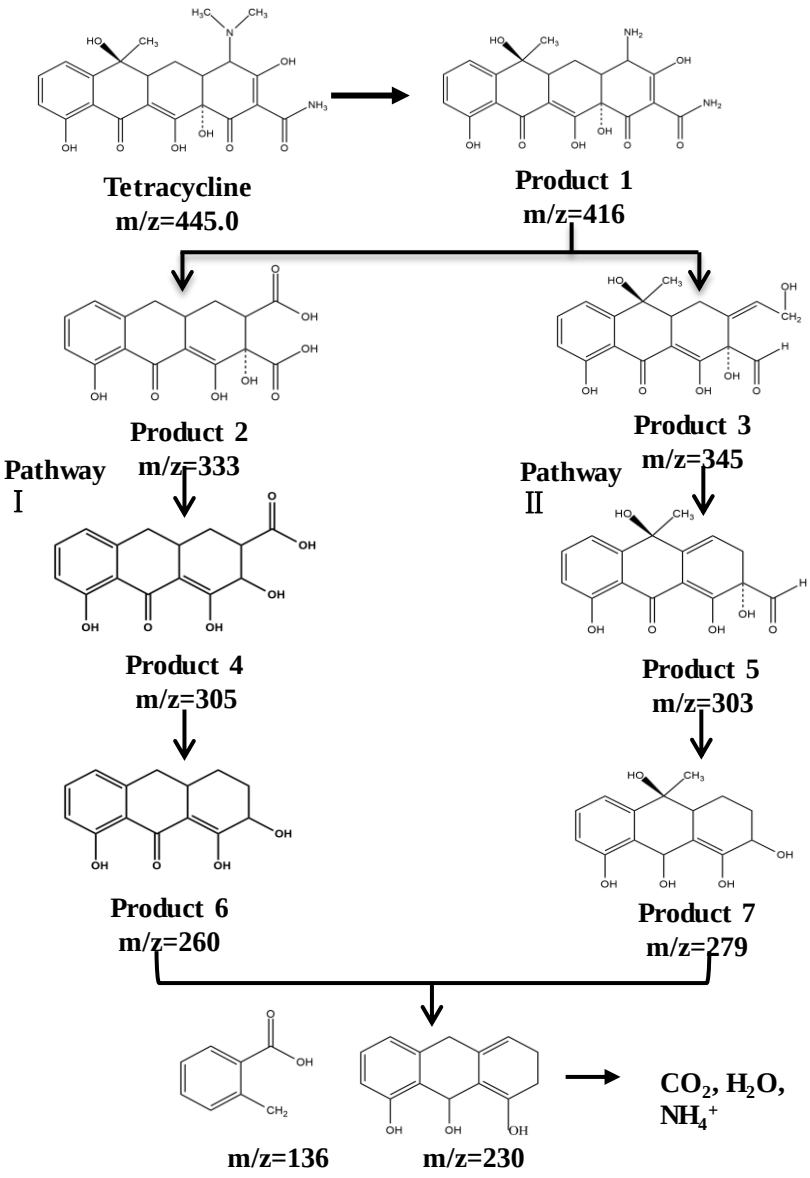

Fig. 11 The proposed photodegradation pathways of TC

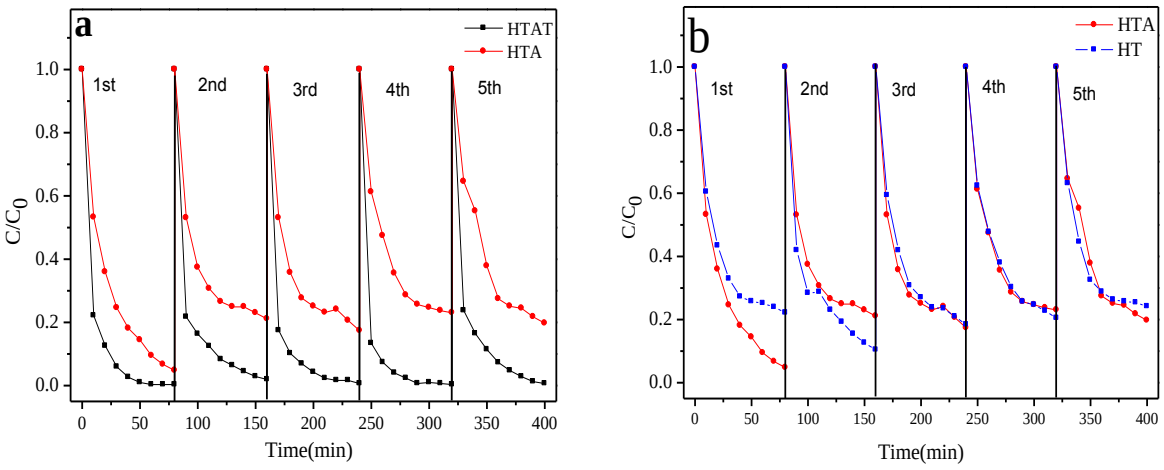

Fig. 12. Cycling tests for the degradation of TC using HTAT, HTA and HT photocatalyst